

Cite this: *Chem. Sci.*, 2024, 15, 3018

All publication charges for this article have been paid for by the Royal Society of Chemistry

# A controlled non-radical chlorine activation pathway on hematite photoanodes for efficient oxidative chlorination reactions†

Daojian Tang,<sup>‡ac</sup> Lei Wu,<sup>‡ac</sup> Liubo Li,<sup>‡ac</sup> Niankai Fu,<sup>bc</sup> Chuncheng Chen,<sup>‡ac</sup> Yuchao Zhang,<sup>‡ac</sup> and Jincai Zhao<sup>‡ac</sup>

Photo(electro)catalytic chlorine oxidation has emerged as a useful method for chemical transformation and environmental remediation. However, the reaction selectivity usually remains low due to the high activity and non-selectivity characteristics of free chlorine radicals. In this study, we report a photoelectrochemical (PEC) strategy for achieving controlled non-radical chlorine activation on hematite ( $\alpha$ -Fe<sub>2</sub>O<sub>3</sub>) photoanodes. High selectivity (up to 99%) and faradaic efficiency (up to 90%) are achieved for the chlorination of a wide range of aromatic compounds and alkenes by using NaCl as the chlorine source, which is distinct from conventional TiO<sub>2</sub> photoanodes. A comprehensive PEC study verifies a non-radical "Cl<sup>+</sup>" formation pathway, which is facilitated by the accumulation of surface-trapped holes on  $\alpha$ -Fe<sub>2</sub>O<sub>3</sub> surfaces. The new understanding of the non-radical Cl<sup>-</sup> activation by semiconductor photoelectrochemistry is expected to provide guidance for conducting selective chlorine atom transfer reactions.

Received 25th November 2023

Accepted 10th January 2024

DOI: 10.1039/d3sc06337b

rsc.li/chemical-science

## Introduction

In the past few decades, solar-driven photo(electro)chemistry has attracted enormous attention for solar fuel production<sup>1–4</sup> and environmental remediation.<sup>5–7</sup> The photoelectrochemical (PEC) technology combines light absorption and electrochemical processes into an integrated unit through direct semiconductor/electrolyte interfaces, offering advantages over particulate photocatalytic systems with its efficient charge separation and collection, as well as easy catalyst recycling.<sup>8,9</sup> In recent years, PEC approaches have pointed towards a more sustainable and energy-saving alternative for redox organic transformations compared to thermal or electrochemical methods in terms of solar energy utilization.<sup>10–13</sup>

Organochlorides are commonly found in many bioactive natural products or synthetic drugs and are widely employed for the construction of complex structures in organic synthesis.<sup>14–17</sup> Conventional synthetic methods involve the use of massive amounts of explosive, corrosive, or toxic chlorine sources such

as chlorine gas (Cl<sub>2</sub>), which raises concerns regarding potential environmental risks.<sup>16,18,19</sup> The electrochemical technology for chlorine evolution has inspired an oxidative chlorination approach to generate reactive chloride species *in situ*, facilitating the green synthesis of high-value chemicals such as chlorohydrins, aryl chlorides, and epoxides.<sup>20–24</sup> Alternatively, PEC-assisted oxidative chlorination is expected to be a clean and more energy-saving chemical process with reduced electrical power input.<sup>25</sup> However, reports on the photoredox protocol for chlorine activation show challenges in PEC oxidative chlorination, where photocatalysts (*e.g.*, TiO<sub>2</sub>,<sup>25–27</sup> WO<sub>3</sub>,<sup>5,6</sup> *etc.*) with deep valence band edges are often used to drive the chloride (Cl<sup>-</sup>) oxidation (Fig. S1†). The photogenerated holes in the valence band (VB) of these photocatalysts are more positive than the 1-e<sup>-</sup> oxidation potential of Cl<sup>-</sup>, which forms chlorine radicals (Cl<sup>•</sup>).<sup>25,27</sup> Although Cl<sup>•</sup> facilitates the activation of C–H bonds,<sup>25,27,28</sup> it can more easily trigger uncontrolled radical chain reactions, leading to polychlorination and radical coupling reactions.<sup>27,29</sup> Thus, a compromise must be made between selectivity and conversion. As such, the development of a PEC approach to achieve more controlled activation of Cl<sup>-</sup> for C–Cl construction remains a substantial challenge.

Hematite ( $\alpha$ -Fe<sub>2</sub>O<sub>3</sub>) is one of the most promising photoanode materials in PEC studies due to its abundance, non-toxicity, stability, and visible light absorption capabilities (Fig. S1†). Recently,  $\alpha$ -Fe<sub>2</sub>O<sub>3</sub> has attracted wide attention for selective oxygen transfer reactions.<sup>30,31</sup> Under PEC conditions, long-lived surface-trapped holes have been demonstrated on  $\alpha$ -Fe<sub>2</sub>O<sub>3</sub>,<sup>32,33</sup> and multi-hole H<sub>2</sub>O oxidation catalysis is realized, in which the

<sup>a</sup>Key Laboratory of Photochemistry, Beijing National Laboratory for Molecular Sciences, Institute of Chemistry, Chinese Academy of Sciences, Beijing 100190, P. R. China. E-mail: yczhang@iccas.ac.cn

<sup>b</sup>Key Laboratory of Molecular Recognition and Function, Beijing National Laboratory for Molecular Sciences, Institute of Chemistry, Chinese Academy of Sciences, Beijing 100190, P. R. China

<sup>c</sup>University of Chinese Academy of Sciences, Beijing 100049, P. R. China

† Electronic supplementary information (ESI) available. See DOI: <https://doi.org/10.1039/d3sc06337b>

‡ These authors contributed equally.



accumulation of multiple oxidizing equivalents (*i.e.*, high-valent iron-oxo species,  $\text{Fe}^{\text{IV}}=\text{O}$  and  $\text{Fe}^{\text{V}}=\text{O}$ ) has been proposed as the key to efficient  $\text{H}_2\text{O}$  oxidation catalysis.<sup>34–36</sup> It is further found that  $\alpha\text{-Fe}_2\text{O}_3$  serves as an efficient oxygen atom transfer (OAT) catalyst, achieving highly selective two-electron oxygenation of substrates such as thioethers and alkenes.<sup>30</sup> The high-valent iron-oxo characteristics of surface-trapped holes on  $\alpha\text{-Fe}_2\text{O}_3$  is reminiscent of the high-valent iron-oxo species in halogenating enzymes, which are capable of controllably oxidizing  $\text{Cl}^-$  to form “ $\text{Cl}^+$ ” species (*e.g.*,  $\text{HClO}$  or its equivalents) through a two-electron oxidation process.<sup>15,37,38</sup> This enables selective electrophilic chlorination for constructing C–Cl bonds and preventing side reactions caused by single-electron radical reactions under relatively mild reaction conditions. There has been a significant advancement in the spectroscopic, physicochemical, and mechanistic investigations of homogeneous Fe catalysts, but the chlorination reaction using heterogeneous Fe or Fe oxide catalysts is rarely reported.<sup>38–40</sup>

Inspired by this, we envision that  $\alpha\text{-Fe}_2\text{O}_3$  could serve as an efficient PEC catalyst for controlled non-radical activation of  $\text{Cl}^-$  for C–Cl construction. In this work, the  $\text{Cl}^-$  oxidation process on  $\alpha\text{-Fe}_2\text{O}_3$  is investigated. We show a direct “ $\text{Cl}^+$ ” species formation process on  $\alpha\text{-Fe}_2\text{O}_3$  surfaces, which is facilitated by the accumulation of surface-trapped holes. As a result,  $\alpha\text{-Fe}_2\text{O}_3$  exhibits a high selectivity (up to 99%) for the synthesis of aromatic chlorides and chlorohydrins. This is in sharp contrast to the low-selective chlorination on  $\text{TiO}_2$  photoanodes, which follows the free radical chlorination pathway. This work is anticipated to offer an in-depth understanding of selective  $\text{Cl}^-$  activation by semiconductor photoelectrochemistry and provide guidance for the construction of efficient chlorine atom transfer reactions.

## Results and discussion

### PEC $\text{Cl}^-$ oxidation behaviors on $\alpha\text{-Fe}_2\text{O}_3$

As a proof of concept, the  $\text{Cl}^-$  activation process on  $\alpha\text{-Fe}_2\text{O}_3$  was firstly investigated.  $\alpha\text{-Fe}_2\text{O}_3$  photoanodes were prepared according to our previous reports.<sup>31</sup> Structural characterization of  $\alpha\text{-Fe}_2\text{O}_3$  is shown in Fig. S2.† The PEC tests were conducted in an H-type cell with a three-electrode configuration, where a Pt wire was used as the cathode and an Ag/AgCl electrode served as the reference electrode. The PEC performance of  $\text{Cl}^-$  oxidation and  $\text{H}_2\text{O}$  oxidation was investigated by using a mixed solution of  $\text{H}_2\text{O}/\text{CH}_3\text{CN}$  ( $v/v = 1:1$ ,  $\text{pH} = 6.4$ ) with 0.1 M NaCl or  $\text{NaClO}_4$  as the electrolyte. Linear sweep voltammetry (LSV) measurements under AM 1.5G irradiation ( $100 \text{ mW cm}^{-2}$ ) exhibited an onset potential of 0.6 V *vs.* Ag/AgCl for oxidizing  $\text{H}_2\text{O}$  in a 0.1 M  $\text{NaClO}_4$  solution on the  $\alpha\text{-Fe}_2\text{O}_3$  photoanode (Fig. 1a). When the electrolyte was replaced with 0.1 M NaCl, the onset potential decreased by approximately 200 mV and the photocurrent was significantly enhanced, indicating that  $\text{Cl}^-$  was preferentially oxidized on  $\alpha\text{-Fe}_2\text{O}_3$ . To further explore the photocurrent behavior, LSV measurements were performed under various concentrations of  $\text{Cl}^-$  solution. As shown in Fig. S3,† the presence of only 10 mM  $\text{Cl}^-$  resulted in a remarkable photocurrent enhancement. Moreover, the overall photocurrent on the  $\alpha\text{-Fe}_2\text{O}_3$

$\text{Fe}_2\text{O}_3$  photoanode increased with the concentration of  $\text{Cl}^-$ , indicating that the enhancement of photocurrent was associated with  $\text{Cl}^-$  oxidation.

Intensity modulated photocurrent spectroscopy (IMPS) measurements were performed to compare interfacial charge-transfer kinetics between the oxidations of  $\text{Cl}^-$  and  $\text{H}_2\text{O}$  on the  $\alpha\text{-Fe}_2\text{O}_3$  photoanode. IMPS plots showed identical semi-circles in the high frequency domain (the fourth quadrant) but a decreased radius of the low-frequency circle in the first quadrant after the addition of  $\text{Cl}^-$  (Fig. S4†). Simulation of the IMPS plots showed that the presence of  $\text{Cl}^-$  increased the charge-transfer rate constant ( $k_{\text{ct}}$ ) from  $13.4 \text{ s}^{-1}$  to  $21.6 \text{ s}^{-1}$  and the charge-transfer efficiency ( $\eta_{\text{ct}}$ ) from 53.5% to 77.0%, indicating that  $\text{Cl}^-$  oxidation was much faster than  $\text{H}_2\text{O}$  oxidation. The inhibition of  $\text{H}_2\text{O}$  oxidation was confirmed by monitoring the generation of  $\text{O}_2$  by gas chromatography (GC, Fig. S5†) after 1 h of photoelectrolysis under AM 1.5G irradiation. As shown in Fig. 1b and Table S1,† the addition of  $\text{Cl}^-$  resulted in a rapid decrease in the faradaic efficiency (FE) of the oxygen evolution reaction (OER) and almost complete suppression when 25–200 mM  $\text{Cl}^-$  was present. To further confirm the high selectivity of  $\text{Cl}^-$  oxidation, we employed the *N,N*-diethyl-*p*-phenylenediamine (DPD) colorimetric method to quantify the active chlorine concentrations under various  $\text{Cl}^-$  solution concentrations (Fig. S6†).<sup>41</sup> The results showed that after 10 min of photoelectrolysis, the FE of active chlorine generation was more than 90% when  $\text{Cl}^-$  concentrations ranged from 25 to 200 mM, which was consistent with the results obtained from OER experiments. In addition, no active chlorination generation was detected under conditions of only electricity or light, suggesting that both light and electricity were necessary in our system for  $\text{Cl}^-$  oxidation (Fig. S7†). Strikingly,  $\alpha\text{-Fe}_2\text{O}_3$  exhibited a high selectivity of  $\text{Cl}^-$  oxidation even at a relatively low  $\text{Cl}^-$  concentration of 50 mM, showing a significant advantage compared to other reported photocatalysts for  $\text{Cl}^-$  oxidation (Table S2†). We also explored the  $\text{Cl}^-$  oxidation performance in an aqueous solution. As shown in Fig. S8,† the selectivity of  $\text{Cl}^-$  oxidation decreased in 0.1 M  $\text{Cl}^-$  aqueous solution compared to that in a  $\text{H}_2\text{O}$ –MeCN mixture solution (Fig. S6†), suggesting that the presence of an organic solvent helped to inhibit the competitive  $\text{H}_2\text{O}$  oxidation reaction. Moreover, a further increase of  $\text{Cl}^-$  concentration could improve the selectivity of  $\text{Cl}^-$  oxidation. Under 0.3 M  $\text{Cl}^-$ , the FE of  $\text{Cl}^-$  oxidation could reach more than 90%, which still showed good selectivity for  $\text{Cl}^-$  oxidation compared to other reported photocatalysts (Table S2†). These results indicated the high reactivity of  $\alpha\text{-Fe}_2\text{O}_3$  towards  $\text{Cl}^-$  oxidation.

Previous research has demonstrated that the process of  $\text{H}_2\text{O}$  oxidation on  $\alpha\text{-Fe}_2\text{O}_3$  occurs through surface-trapped holes rather than direct hole transfer from the valence band.<sup>42,43</sup> In order to uncover the underlying relationship between the  $\text{Cl}^-$  oxidation and the surface-trapped holes, electrochemical impedance spectroscopy (EIS) measurements were carried out under the same conditions to investigate the interface reaction of  $\text{Cl}^-$  oxidation and  $\text{H}_2\text{O}$  oxidation on  $\alpha\text{-Fe}_2\text{O}_3$ . As shown in Fig. 1c, the Nyquist plots for both  $\text{Cl}^-$  oxidation and  $\text{H}_2\text{O}$  oxidation on the  $\alpha\text{-Fe}_2\text{O}_3$  photoanode consisted of two

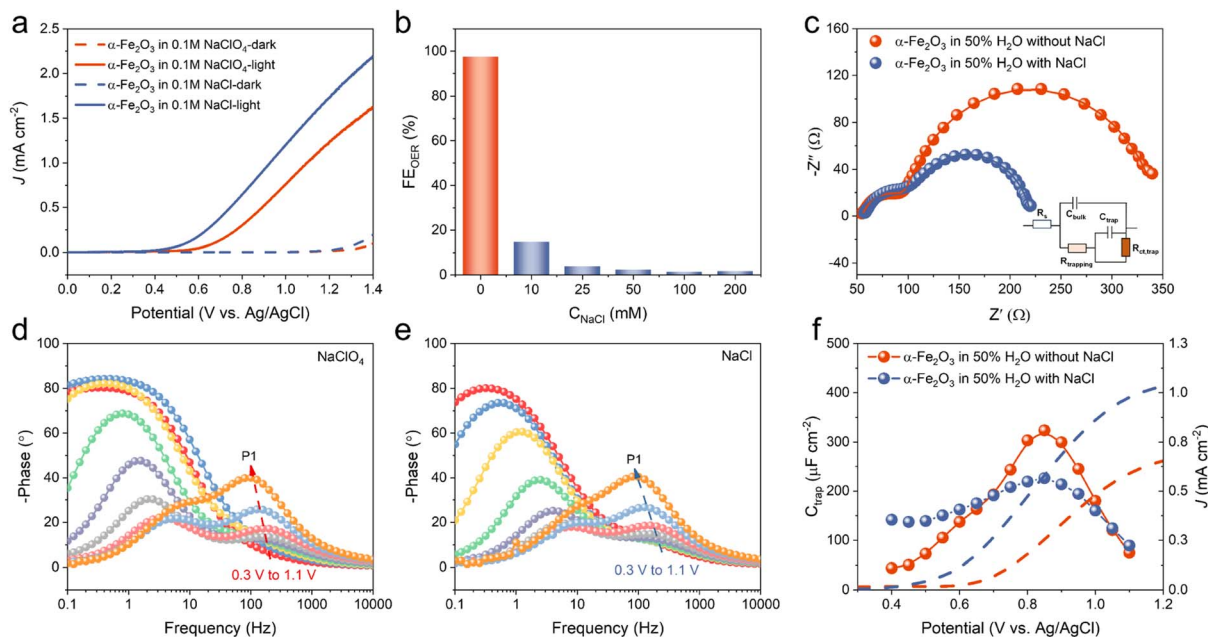


**Fig. 1** PEC  $\text{Cl}^-$  oxidation activity and reaction kinetics on  $\alpha\text{-Fe}_2\text{O}_3$  photoanodes. (a) LSV curves of an  $\alpha\text{-Fe}_2\text{O}_3$  photoanode in a mixed solution of  $\text{CH}_3\text{CN}/\text{H}_2\text{O}$  (1 : 1 v/v) with 0.1 M  $\text{NaClO}_4$  or  $\text{NaCl}$  as the electrolyte under AM 1.5G irradiation. (b) The FE of the OER after 1 h of photoelectrolysis at 1.0 V vs. Ag/AgCl with different concentrations of  $\text{Cl}^-$ . (c) Nyquist plots and the fitted curves of an  $\alpha\text{-Fe}_2\text{O}_3$  photoanode in 0.1 M  $\text{NaClO}_4$  solution with or without 10 mM  $\text{Cl}^-$  under 470 nm irradiation at 1.0 V vs. Ag/AgCl. The inset is the equivalent circuit for EIS fitting. (d) Potential-dependent Bode plots measured in 0.1 M  $\text{NaClO}_4$  solution; (e) potential-dependent Bode plots measured in 0.1 M  $\text{NaClO}_4$  solution with 10 mM  $\text{Cl}^-$ . (f) LSV curves (dashed lines) and  $C_{\text{trap}}$  values (solid lines and dots) obtained on an  $\alpha\text{-Fe}_2\text{O}_3$  photoanode with 10 mM  $\text{Cl}^-$  (grayish blue) and without  $\text{Cl}^-$  (red) under 470 nm irradiation.

semicircles, and its Bode plots exhibited two peaks at different frequency regions (Fig. 1d and e). This is a typical feature of surface-state mediated charge transfer rather than direct hole transfer.<sup>3,43</sup> The high-frequency (HF) semicircle in Nyquist plots should be assigned to the surface hole-trapping process and the low-frequency (LF) semicircle should be attributed to the transfer of those trapped holes to the electrolyte. In Fig. 1c, the HF semicircles were almost unchanged upon adding 10 mM  $\text{Cl}^-$ , which indicated that  $\text{Cl}^-$  had little effect on the generation of surface trapped holes. To further confirm this, potential-dependent experiments were conducted. For both  $\text{H}_2\text{O}$  oxidation and  $\text{Cl}^-$  oxidation, the potential-dependent experiments (Fig. 1d and e) showed the phase angle of the HF region (P1, which was assigned to the surface hole-trapping process) in Bode plots increased with applied potentials, suggesting the accumulation of surface-trapped holes. Regardless of the presence of  $\text{Cl}^-$ , there was no distinction in the phase angle P1, demonstrating that  $\text{Cl}^-$  oxidation and  $\text{H}_2\text{O}$  oxidation shared similar surface states or active sites. This was consistent with the competitive oxidation process of  $\text{Cl}^-$  and  $\text{H}_2\text{O}$  (Fig. 1b and S6†). The trapped holes on these surface states were previously assigned to high-valent surface iron-oxo species, *i.e.*,  $\text{Fe}^{\text{IV}}=\text{O}$  and  $\text{Fe}^{\text{V}}=\text{O}$ .<sup>43,44</sup> On the other hand, compared to  $\text{H}_2\text{O}$  oxidation, the radius of the LF semicircle in  $\text{Cl}^-$  oxidation was significantly reduced (Fig. 1c). This demonstrated that the oxidation of  $\text{Cl}^-$  mediated by surface-trapped holes was easier than the oxidation of  $\text{H}_2\text{O}$ , which correlated well with the increasing photocurrent and the IMPS results.

To quantify the two associated capacitive elements, a well-established physical model consisting of the space-charge capacitance ( $C_{\text{bulk}}$ ) and surface-state capacitance ( $C_{\text{trap}}$ ) was considered (see details in Fig. S9†).<sup>3,43–45</sup> As shown in Fig. 1f, in 0.1 M  $\text{NaClO}_4$  solution, the fitted  $C_{\text{trap}}$  increased with the applied bias at low potentials and reached a maximum at approximately 0.85 V due to the accumulation of surface-trapped holes. After that,  $C_{\text{trap}}$  began to decrease because of the increased consumption rate of surface-trapped holes. In the presence of  $\text{Cl}^-$ , the maximum value of  $C_{\text{trap}}$  was smaller than that in the 0.1 M  $\text{NaClO}_4$  solution, indicating that the consumption of surface-trapped holes by  $\text{Cl}^-$  oxidation were faster than that by  $\text{H}_2\text{O}$  oxidation. To further prove that  $\text{Cl}^-$  oxidation was mediated by the high-valent iron-oxo species, the behavior of surface-state capacitance ( $C_{\text{trap}}$ ) with  $\text{Cl}^-$  concentrations was investigated (Fig. S10†). The  $C_{\text{trap}}$  values decreased with the concentration of  $\text{Cl}^-$ , supporting that  $\text{Cl}^-$  oxidation was favorably mediated by the high-valent iron-oxo species. Therefore, we anticipated an efficient PEC chlorination of  $\alpha\text{-Fe}_2\text{O}_3$  through a controlled non-radical  $\text{Cl}^-$  activation pathway similar to that of halogenating enzymes.

### Different oxidative chlorination behaviors on $\alpha\text{-Fe}_2\text{O}_3$ and $\text{TiO}_2$

Aromatic chlorides are widely applied in pharmaceuticals, agrochemicals, and organic materials for modifying their biological or physicochemical properties.<sup>14,15</sup> They also serve as important starting materials for cross-coupling reactions.<sup>18</sup> It is

reported that aromatic chlorination can be efficiently driven *via* a non-radical electrophilic chlorination reaction.<sup>18,46</sup> Therefore, aromatic chlorination of acetanilide (**1a**) was chosen as one model reaction to explore PEC oxidative chlorination (Fig. 2a, model reaction I). LSV measurements in Fig. S11† showed that, under AM 1.5 G irradiation, the presence of **1a** did not change the onset potential and the photocurrent in the whole tested voltage range of 0.0 to 1.2 V vs. Ag/AgCl (red dash curves), which suggested that the direct oxidation of **1a** should not occur on  $\alpha$ -Fe<sub>2</sub>O<sub>3</sub>. To further confirm this, the Cl<sup>-</sup> oxidation and **1a** oxidation were compared in a 100% MeCN solution with NEt<sub>4</sub>BF<sub>4</sub> as the supporting electrolyte. As shown in Fig S12,† we observed that the direct oxidation of **1a** occurred at higher overpotentials. Moreover, compared with Cl<sup>-</sup> oxidation, the onset potential of **1a** oxidation anodically shifted by 0.4 V on the  $\alpha$ -Fe<sub>2</sub>O<sub>3</sub> photoanode, suggesting that the direct oxidation of **1a** on  $\alpha$ -Fe<sub>2</sub>O<sub>3</sub> in the oxidative chlorination reaction system would be difficult to occur. This excluded the possibility that the chlorination reaction was conducted through activation of **1a** to yield the chlorination products.

To investigate the performance of aromatic chlorination on  $\alpha$ -Fe<sub>2</sub>O<sub>3</sub>, chronoamperometry was conducted at 1.0 V vs. Ag/AgCl under AM 1.5G irradiation for 2 h under the same conditions. Product analysis by high-performance liquid chromatography (HPLC) showed that **1a** was converted into chlorinated products **2a** and **3a** (Fig. S13†). The FE for chlorinated products **2a** and **3a** on the  $\alpha$ -Fe<sub>2</sub>O<sub>3</sub> photoanode was found to be 90%, with a remarkable selectivity of 98% for monochlorinated product **2a**

(*p/o* = 1.6 : 1) (Fig. 2b). It has been reported that the TiO<sub>2</sub> photoanodes drive Cl<sup>-</sup> oxidation to form <sup>•</sup>Cl through a single-electron oxidation mechanism.<sup>25</sup> To confirm the uniqueness of  $\alpha$ -Fe<sub>2</sub>O<sub>3</sub> for efficient aromatic chlorination, the oxidative chlorination of **1a** on a TiO<sub>2</sub> photoanode was investigated and compared with that on  $\alpha$ -Fe<sub>2</sub>O<sub>3</sub>. Structural characterization of TiO<sub>2</sub> is shown in Fig. S14.† The FE for aromatic chlorination of **1a** on TiO<sub>2</sub> was only 50%, while the selectivity for **2a** was 57% (Fig. 2b). In addition, the TiO<sub>2</sub> photoanode showed a higher **3a**/**2a** ratio for chlorinated products compared to that on the  $\alpha$ -Fe<sub>2</sub>O<sub>3</sub> photoanode, suggesting a low regioselectivity for aromatic mono-chlorination. This was consistent with the polychlorination occurring during the <sup>•</sup>Cl-involved chlorination reaction. Potential-dependent experiments on the  $\alpha$ -Fe<sub>2</sub>O<sub>3</sub> photoanode revealed that a high FE (>90%) was maintained within the potential range of 0.7 to 1.0 V (Fig. S15a†). By extending the electrolysis time to 2.5 h, a yield of 95% for **2a** was achieved on the  $\alpha$ -Fe<sub>2</sub>O<sub>3</sub> photoanode (Fig. S15b†). We evaluated the stability of the  $\alpha$ -Fe<sub>2</sub>O<sub>3</sub> photoanode in batch reactions. Under high conversion of the substrate (>90%), a high selectivity of 98% was maintained for the 6th run under the same reaction conditions (Fig. 2c). The X-ray diffraction (XRD), X-ray absorption fine structure spectra (XAFS) and X-ray photoelectron spectroscopy (XPS) characterizations (Fig. S16 and 17†) displayed no changes for the used  $\alpha$ -Fe<sub>2</sub>O<sub>3</sub>, demonstrating the stability of  $\alpha$ -Fe<sub>2</sub>O<sub>3</sub>. Moreover, the presence of obvious Cl<sup>-</sup> residues was observed after photoelectrolysis, indicating a strong absorption of Cl<sup>-</sup> on Fe<sub>2</sub>O<sub>3</sub> surfaces (Fig. S17c and d†).

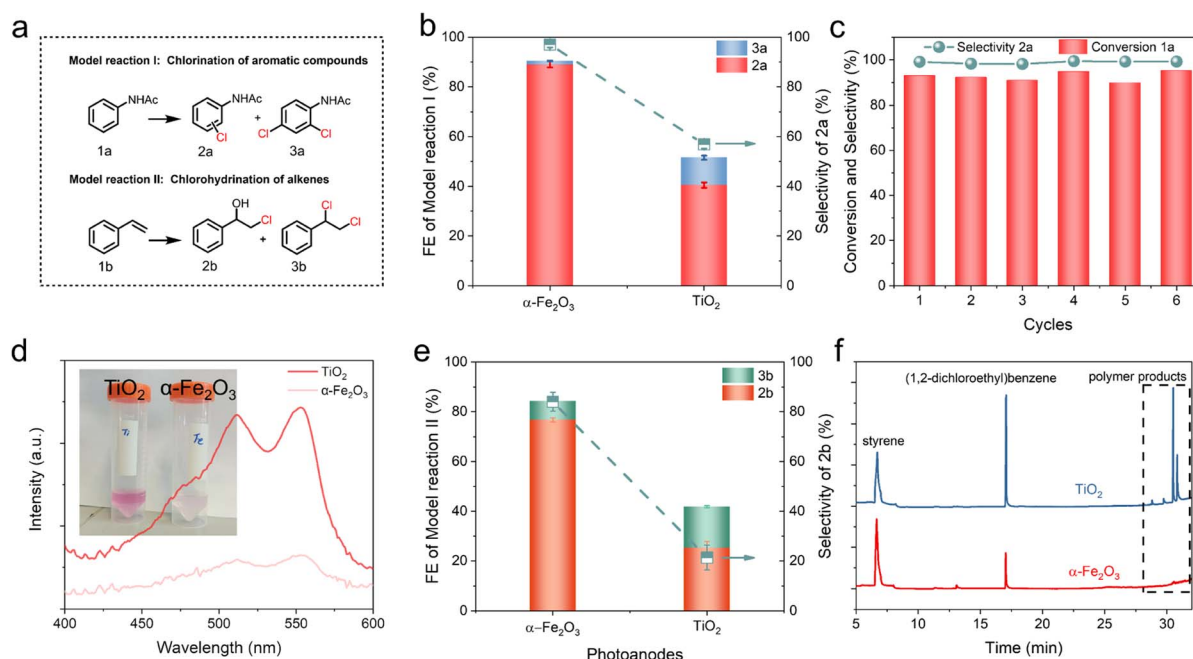


**Fig. 2** Photoelectrolysis experiments of PEC oxidative chlorination. (a) The model reactions for the PEC oxidative chlorination reaction. (b) The aromatic chlorination activity compared on  $\alpha$ -Fe<sub>2</sub>O<sub>3</sub> and TiO<sub>2</sub>. (c) The cyclic stability test of a single  $\alpha$ -Fe<sub>2</sub>O<sub>3</sub> photoanode in 0.1 M NaCl with 10 mM **1a** at 1.0 V vs. Ag/AgCl. (d) The UV-vis spectra of DPD colorimetric tests for the detection of active chlorine derivatives during aromatic chlorination on  $\alpha$ -Fe<sub>2</sub>O<sub>3</sub> and TiO<sub>2</sub> after 2 h of photoelectrolysis at 1.0 V vs. Ag/AgCl. Inset: the digital photograph of the anolyte with DPD test solution added. (e) FE and selectivity for the chlorohydrin product on  $\alpha$ -Fe<sub>2</sub>O<sub>3</sub> and TiO<sub>2</sub> after 2 h of photoelectrolysis at 1.0 V vs. Ag/AgCl in 0.1 M NaCl solution. (f) The GC-MS spectra of styrene chlorination products on  $\alpha$ -Fe<sub>2</sub>O<sub>3</sub> and TiO<sub>2</sub> after 1 h of photoelectrolysis.

More importantly, the enhanced interfacial charge transfer of  $\text{Cl}^-$  oxidation resulted in a higher solar  $\text{H}_2$  production ( $47 \mu\text{mol h}^{-1}$ ) compared to  $\text{H}_2\text{O}$  oxidation ( $22 \mu\text{mol h}^{-1}$ ) as the oxidative half reaction (Fig. S18†), suggesting a higher utilization efficiency of photo-induced charges and a more effective storage of solar energy through the coupled electrophilic chlorination reaction with  $\text{H}_2$  production.

Considering the high  $\text{Cl}^-$  oxidation performance across a wide range of  $\text{Cl}^-$  concentrations (10–200 mM, Fig. 1b and S6†), the aromatic chlorination of **1a** with different  $\text{Cl}^-$  concentrations was also evaluated. At the same potential (1.0 V vs. Ag/AgCl), the yield rate of **2a** increased with the higher concentration of  $\text{Cl}^-$ , reaching  $23 \mu\text{mol cm}^{-2} \text{h}^{-1}$ , while the selectivity of **2a** remained up to 90% (Fig. S15c and d†). This was consistent with the linear change in  $\text{Cl}^-$  oxidation photocurrent (Fig. S3b†), indicating that the rate-determining step (RDS) of aromatic chlorination was the PEC  $\text{Cl}^-$  oxidation rather than the subsequent chemical process. More importantly, under low  $\text{Cl}^-$  concentration (10 mM  $\text{Cl}^-$ , 1 equiv. substrate concentration), the chlorination activity on the  $\alpha\text{-Fe}_2\text{O}_3$  photoanode still showed a high FE of 75%, indicating the efficient  $\text{Cl}^-$  oxidation and the rapid aromatic chlorination process on the  $\alpha\text{-Fe}_2\text{O}_3$  photoanode. The effective chlorination process on the  $\alpha\text{-Fe}_2\text{O}_3$  photoanode was also supported by inhibiting the further oxidation of active chlorine species to form  $\text{ClO}_3^-$  (Fig. S19†). During photoelectrolysis without **1a**, the analysis of  $\text{Cl}^-$  oxidation products using ion chromatography (IC) showed a gradual accumulation of  $\text{ClO}_3^-$  over a period of 2 h (Fig. S19a†). However, when photoelectrolysis was performed in the presence of **1a**,  $\text{ClO}_3^-$  formation was completely inhibited (Fig. S19b†) and the chlorination of **1a** showed a high current efficiency (FE 98%), indicating the rapid reaction between **1a** and active chlorine species. This was further supported by DPD colorimetric tests,<sup>41</sup> in which most of the active chlorine species derived from  $\text{Cl}^-$  oxidation already participated in the aromatic chlorination and only a small portion of them was residual and detected on the  $\alpha\text{-Fe}_2\text{O}_3$  photoanode (Fig. 2d). In contrast, DPD colorimetric tests showed a significant accumulation of active chlorine species on the  $\text{TiO}_2$  photoanode (Fig. 2d), suggesting that most of the active chlorine species generated from  $\text{Cl}^-$  oxidation on  $\text{TiO}_2$  were unable to participate in the subsequent aromatic chlorination and were thus detected by DPD tests.  $\cdot\text{Cl}$  can lead to uncontrolled hydrogen abstraction and polymerization reactions, resulting in the low aromatic chlorination activity.<sup>18</sup> These results suggested that PEC activation of  $\text{Cl}^-$  on  $\alpha\text{-Fe}_2\text{O}_3$  and  $\text{TiO}_2$  photoanodes produced distinct active chlorine species.

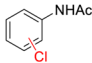
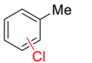
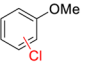
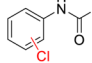
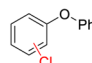
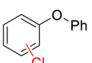
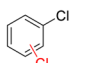
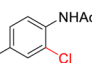
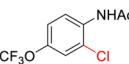
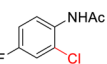
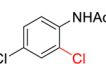
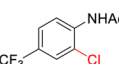
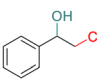
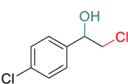
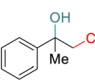
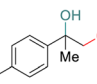
To further confirm this, we explored the synthesis of chlorohydrin products (Fig. 2a, model reaction II), which act as essential intermediates in industrial-scale epoxidations.  $\cdot\text{Cl}$  can initiate radical chain reactions or radical coupling reactions, resulting in the formation of dimeric or polymeric products during the chlorination of alkene.<sup>47,48</sup> After electrolysis at 1.0 V vs. Ag/AgCl for 2 h, product analysis by HPLC showed that nearly 80% conversion of **1b** with up to 85% selectivity of chlorohydrin **2b** was achieved on the  $\alpha\text{-Fe}_2\text{O}_3$  photoanode (Fig. 2e and S20†). The calculated FE was close to

80%. In addition to producing chlorohydrin products of **2b**, a minor quantity of dichloride products of **3b** was also observed (Fig. 2e). In contrast, the chlorohydrin of **1b** on the  $\text{TiO}_2$  photoanode only exhibited an FE of 23% and a selectivity of 21% for **2b**. It also showed a much higher production of dichlorination products **3b** (Fig. 2e). The gas chromatography-mass spectrometry (GC-MS, Fig. 2f) revealed the formation of high molecular mass polymers on the  $\text{TiO}_2$  photoanode, which were not observed on the  $\alpha\text{-Fe}_2\text{O}_3$  photoanode. These results indicated that  $\cdot\text{Cl}$  is not formed and the selective electrophilic chlorination process occurs on  $\alpha\text{-Fe}_2\text{O}_3$ .

### Scope of PEC oxidative chlorination on $\alpha\text{-Fe}_2\text{O}_3$

To show the general applicability of the PEC strategy for controlled oxidative chlorination on the  $\alpha\text{-Fe}_2\text{O}_3$  photoanode, a broad scope of substrates was tested. We first explored mono-substituted aromatic compounds. As shown in Table 1, aromatic compounds with strong electron-donating groups on the phenyl ring, such as methyl (**2**), methoxyl (**3**), benzamide (**4**), and ether (**5**), exhibited good regioselectivity towards mono-chlorination products. After 2 h of photoelectrolysis, both *para*-

**Table 1** Scope of PEC oxidative chlorination reactions on  $\alpha\text{-Fe}_2\text{O}_3$  photoanodes

Aromatic chlorination products			
			
<b>1<sup>a</sup></b> , con. 83%, sel. 98%, ( <i>p</i> / <i>o</i> =1.6:1)	<b>2<sup>a</sup></b> , con. 76%, sel. 95%, ( <i>p</i> / <i>o</i> =1:1.6)	<b>3<sup>a</sup></b> , con. 65%, sel. 99%, ( <i>p</i> / <i>o</i> =2.6:1)	<b>4<sup>a</sup></b> , con. 59%, sel. 95%, ( <i>p</i> / <i>o</i> =1.8:1)
			
<b>5<sup>a</sup></b> , con. 41%, sel. 98%, ( <i>p</i> / <i>o</i> =3.9:1)	<b>5<sup>b</sup></b> , con. 85%, sel. 79%, ( <i>p</i> / <i>o</i> =5.8:1)	<b>6<sup>a</sup></b> , con. <4%	<b>7<sup>a</sup></b> , con. 89%, sel. 87%
			
<b>8<sup>a</sup></b> , con. 86%, sel. > 99%	<b>9<sup>a</sup></b> , con. 81%, sel. > 99%	<b>10<sup>a</sup></b> , con. 82%, sel. > 99%	<b>11<sup>a</sup></b> , con. 76%, sel. > 99%
Chlorohydrin products			
			
<b>12<sup>a</sup></b> , con. 80%, sel. 84%	<b>13<sup>a</sup></b> , con. 91%, sel. 74%	<b>14<sup>a</sup></b> , con. 89%, sel. 74%	<b>15<sup>a</sup></b> , con. 87%, sel. 74%

<sup>a</sup> typical reaction conditions applied in this work: 0.1 M NaCl, 0.1 mmol substrate in 10 mL of  $\text{CH}_3\text{CN}$  solution with 50%  $\text{H}_2\text{O}$  (*v/v* = 1 : 1), PEC reactions were carried out for 2 h under AM 1.5G irradiation at 1.0 V vs. Ag/AgCl with a non-conditioned air atmosphere and pH adjustments. <sup>b</sup> reaction in 0.1 M  $\text{NET}_4\text{BF}_4$  with 16%  $\text{H}_2\text{O}$  and 50 mM NaCl for 2 h. <sup>c</sup> reaction in 0.1 M  $\text{NET}_4\text{BF}_4$  with 16%  $\text{H}_2\text{O}$  and 50 mM NaCl for 5 h.

and *ortho*-chlorinated products were formed (Fig. S21–24†). However, due to the limited solubility of substrates 4 and 5 in the 50% H<sub>2</sub>O of MeCN solution, the conversion rate was low. When the chlorination reaction was conducted in the 16% H<sub>2</sub>O of MeCN solution, substrate 5 exhibited a high conversion with a selectivity of 79% for monochlorination products (Fig. S24†). Moreover, the substrate that only contained an electron-withdrawing group (chlorine, 6) did not undergo chlorination. This was consistent with the limitations of electrophilic chlorination, in which electrophilic “Cl<sup>+</sup>” species were the major reagent for the chlorination process. Although mono-substituted substrates were chlorinated at both the *ortho* and *para* positions due to the inherent reactivity of “Cl<sup>+</sup>” species, complete site selectivity can be achieved for disubstituted substrates. In these cases, chlorination occurred exclusively *ortho* to the amide group. Substrates bearing functional groups with various electron-rich and electron-deficient substituents, including methyl (7), trifluoromethoxy (8), halogen (9–10), and trifluoromethyl (11), were all chlorinated in good yields as well (Fig. S25–29†).

In addition, the electrosynthesis of chlorohydrins was explored. As shown in Table 1, our PEC approach exhibited a high yield for the chlorohydration of styrene and its derivatives (12–15) (Fig. S30–32†), thus demonstrating the universality of the PEC halogenation strategy on  $\alpha$ -Fe<sub>2</sub>O<sub>3</sub> photoanodes for conducting efficient chlorine atom transfer reactions.

### Direct “Cl<sup>+</sup>” formation on $\alpha$ -Fe<sub>2</sub>O<sub>3</sub>

DPD tests showed an efficient chlorine transfer process on  $\alpha$ -Fe<sub>2</sub>O<sub>3</sub> (Fig. 2d). The highly selective formation of the “Cl<sup>+</sup>” species is essential for effective electrophilic chlorination.<sup>46</sup> Many efforts have pointed out that the surface-trapped holes on  $\alpha$ -Fe<sub>2</sub>O<sub>3</sub> facilitate the non-radical multi-hole oxidation process.<sup>30,31</sup> We hypothesized that  $\alpha$ -Fe<sub>2</sub>O<sub>3</sub> surfaces could potentially facilitate a “Cl<sup>+</sup>” species formation pathway, which would be responsible for the selective electrophilic chlorination of aromatic compounds and alkenes.

Based on the kinetics of various mono-substituted benzene substrates in the aromatic chlorination reaction, the Hammett linear free energy relationship can be calculated. It showed a negative slope of  $-1.1$  for *para*-chlorinated products on the  $\alpha$ -Fe<sub>2</sub>O<sub>3</sub> photoanode (Fig. 3a), indicating the positive charge buildup at the aromatic moiety of the substrate in the transition state. This confirmed the electrophilic chlorination pathway mediated by non-radical “Cl<sup>+</sup>” species on  $\alpha$ -Fe<sub>2</sub>O<sub>3</sub> photoanodes. This was further supported by toluene chlorination experiments (Fig. 3b). The “Cl<sup>+</sup>” species only triggers electrophilic aromatic substitution reactions, while highly reactive  $\cdot$ Cl easily induces competitive sp<sup>3</sup> C–H chlorination, resulting in low selectivity during the  $\cdot$ Cl-mediated aromatic chlorination process (Fig. S33†). As shown in Fig. 3b, TiO<sub>2</sub> generated few aromatic chlorination products (chlorotoluene, CT) in toluene chlorination experiments, but mainly produced the sp<sup>3</sup> C–H chlorination product benzyl chloride (BC). In contrast, the  $\alpha$ -Fe<sub>2</sub>O<sub>3</sub> photoanode exhibited a high CT yield rate of 12.6  $\mu\text{mol cm}^{-2} \text{h}^{-1}$  at 1.0 V vs. Ag/AgCl (Fig. 3b),

suggesting that  $\cdot$ Cl was the main active chlorine species on the TiO<sub>2</sub>, while the active chlorine species generated on the  $\alpha$ -Fe<sub>2</sub>O<sub>3</sub> were more likely to be “Cl<sup>+</sup>” species rather than  $\cdot$ Cl. To further confirm this, electron paramagnetic resonance (EPR) measurements were carried out to detect possible radicals. 5,5-Dimethyl-1-pyrroline *N*-oxide (DMPO) was used as the spin-trapping reagent to capture the possible radicals that were generated in the photoelectrolysis. As shown in Fig. 3c, radical signals were detected only on the TiO<sub>2</sub> photoanode. The three peaks at 3338, 3353, and 3368 G were attributed to DMPO-Cl $\cdot$ , which was *in situ* produced by the reaction between DMPO and Cl $\cdot$  during the photoelectrolysis on TiO<sub>2</sub> (red rhombi). The quartet peaks at 3332, 3345, 3360, and 3374 G with an intensity ratio of 1 : 2 : 2 : 1 corresponded to DMPO-OH $\cdot$  (yellow stars). The other six peaks indicated the formation of DMPO-OCl $\cdot$  (blue hearts).<sup>49,50</sup> These EPR experiments supported the radical process on TiO<sub>2</sub> and non-radical process on  $\alpha$ -Fe<sub>2</sub>O<sub>3</sub>.

Cl<sub>2</sub> is also one of the active chlorine species and can be formed by the self-coupling of Cl $\cdot$ . To rule out the possibility that Cl<sub>2</sub> is the main active chlorine species on  $\alpha$ -Fe<sub>2</sub>O<sub>3</sub>, substrate generation/tip collection mode scanning electrochemical microscopy (SG/TC SECM) measurements were conducted (see more details in Fig. S35 and S36†) to directly monitor the formation of Cl<sub>2</sub> on the photoanodes surfaces. As shown in Fig. 3d, Cl<sub>2</sub> was used as the probe molecule to specifically detect Cl<sub>2</sub> generated from the photoanode surface at an ultra-close distance ( $\sim 13 \mu\text{m}$ ). With the increase in photocurrent ( $I_{\text{sub}}$ ) after an onset potential of  $-0.2 \text{ V vs. Ag/AgCl}$ , the corresponding rise in  $I_{\text{tip}}$  unequivocally confirmed the formation of Cl<sub>2</sub> on TiO<sub>2</sub> surfaces (Fig. 3e). In contrast, the production of Cl<sub>2</sub> was significantly lower on  $\alpha$ -Fe<sub>2</sub>O<sub>3</sub> surfaces, especially when the applied potential exceeded 0.9 V vs. Ag/AgCl. For example, at 1.2 V vs. Ag/AgCl, the  $I_{\text{sub}}$  for Cl $\cdot$  oxidation on  $\alpha$ -Fe<sub>2</sub>O<sub>3</sub> was significantly higher than that on TiO<sub>2</sub>. In contrast, the  $I_{\text{tip}}$  for Cl<sub>2</sub> production was more than 4 times lower on  $\alpha$ -Fe<sub>2</sub>O<sub>3</sub> compared to that on TiO<sub>2</sub>, demonstrating that Cl<sub>2</sub> was not the main product on  $\alpha$ -Fe<sub>2</sub>O<sub>3</sub> surfaces. The residue amount of Cl<sub>2</sub> on  $\alpha$ -Fe<sub>2</sub>O<sub>3</sub> may originate from the reaction between “Cl<sup>+</sup>” species and Cl $\cdot$ .

To further explore the nature of the Cl $\cdot$  activation process on  $\alpha$ -Fe<sub>2</sub>O<sub>3</sub>, rate law analysis based on EIS measurements was performed to compare the hole transfer kinetics for Cl $\cdot$  oxidation between  $\alpha$ -Fe<sub>2</sub>O<sub>3</sub> and TiO<sub>2</sub> photoanodes (see details in Fig. S9†). Cl $\cdot$  oxidation on  $\alpha$ -Fe<sub>2</sub>O<sub>3</sub> showed a second-order kinetics (Fig. 3f and S37, and Tables S4 and S5†). In contrast, Cl $\cdot$  oxidation on TiO<sub>2</sub> exhibited a first-order kinetics. The second-order reaction kinetics indicated that two-hole transfer was involved in the RDS for the Cl $\cdot$  oxidation reaction on  $\alpha$ -Fe<sub>2</sub>O<sub>3</sub>, indicating that “Cl<sup>+</sup>” species were directly formed from the reaction between the absorbed Cl $\cdot$  and the surface-trapped holes (*i.e.*, high-valent iron-oxo species). To support this conclusion, HClO was purposely used as a model “Cl<sup>+</sup>” reagent for the chlorination of 1a. As shown in Fig. S38,† its product distribution was similar to that under the PEC reaction conditions, implying that “Cl<sup>+</sup>” species (*e.g.*, HClO or its equivalents) were the actual active chlorine species during the PEC Cl $\cdot$

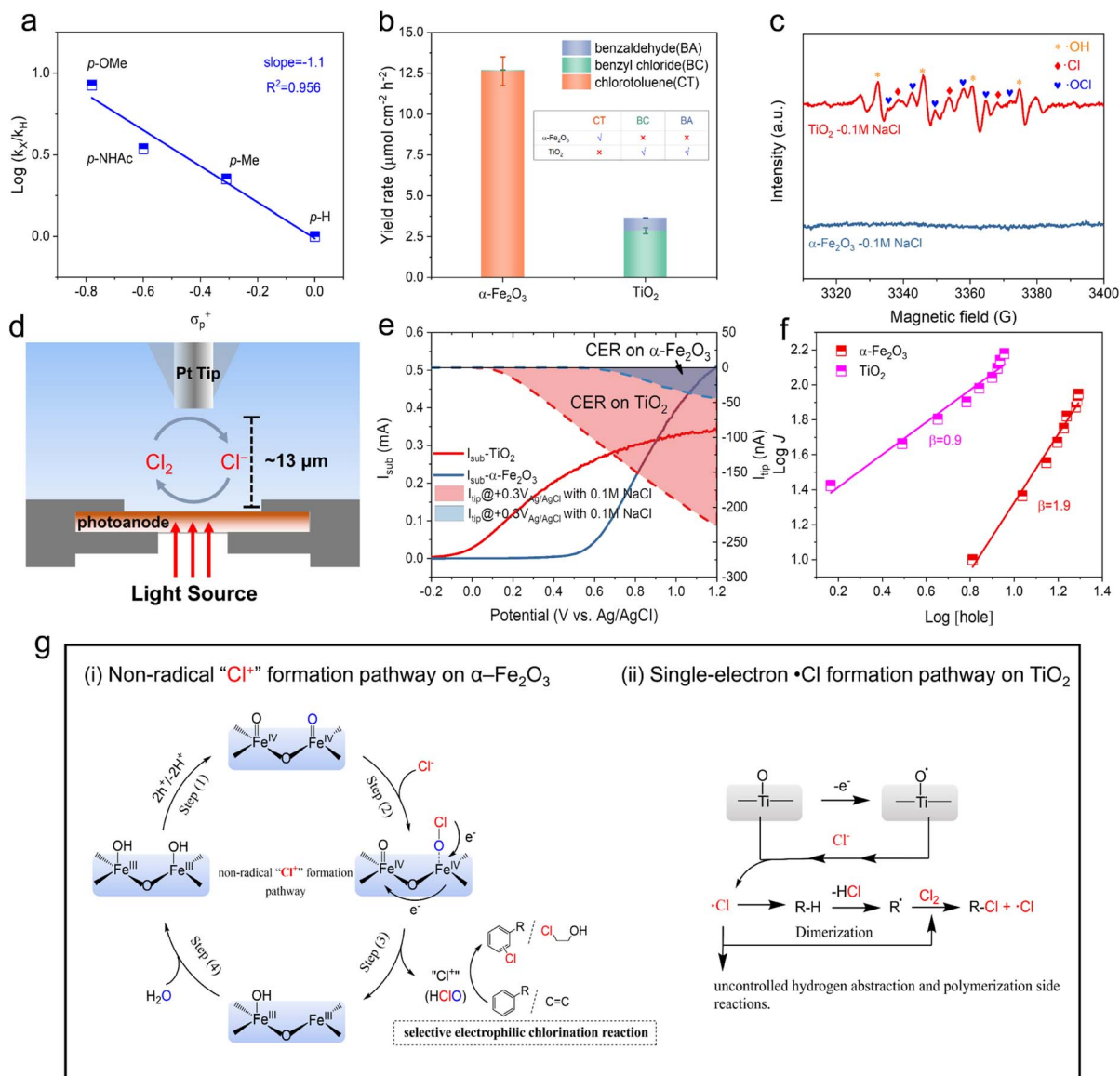


**Fig. 3** Different  $\text{Cl}^-$  activation behaviors on  $\alpha\text{-Fe}_2\text{O}_3$  and  $\text{TiO}_2$ . (a) Hammett plot for the *para*-chlorination of mono-substituted benzene on  $\alpha\text{-Fe}_2\text{O}_3$ . (b) Toluene chlorination experiments for  $\alpha\text{-Fe}_2\text{O}_3$  and  $\text{TiO}_2$ . (c) EPR spectra of the solution obtained from an *in situ* trapping method during PEC  $\text{Cl}^-$  oxidation on  $\text{TiO}_2$  and  $\alpha\text{-Fe}_2\text{O}_3$ , with the addition of DMPO as a radical capture reagent. (d) Schematic of SG/TC SECM experiments. (e) The substrate current and the tip current during LSV ( $5\text{ mV s}^{-1}$ ) for  $\text{Cl}^-$  oxidation on  $\alpha\text{-Fe}_2\text{O}_3$  and  $\text{TiO}_2$ . (f) Rate law analysis for  $\text{Cl}^-$  oxidation on  $\alpha\text{-Fe}_2\text{O}_3$  and  $\text{TiO}_2$ . (g) Schematic illustration for distinct PEC oxidative chlorination reaction pathways on  $\alpha\text{-Fe}_2\text{O}_3$  and  $\text{TiO}_2$ .

oxidation on  $\alpha\text{-Fe}_2\text{O}_3$  for the subsequent electrophilic chlorination. In contrast, the  $\text{Cl}^-$  oxidation on  $\text{TiO}_2$  was dominated by transfer of a single surface-trapped hole, which is consistent with the free radical characteristics of  $\text{TiO}_2$ .

### The proposed mechanism

According to the above results, the proposed reaction mechanism was summarized in Fig. 3g. The formation of surface-trapped holes is believed to occur through hole transfers to hydroxyl groups coordinated on the surface, accompanied by a simultaneous deprotonation step (step 1).<sup>44,51</sup> The trapping of holes could lead to the formation of the two adjacent high-valent surface iron-oxo species (see details in Fig. S39<sup>†</sup>). After

the formation of surface-trapped holes, as indicated by EIS analysis (Fig. 1c and f), the nucleophilic attack of a  $\text{Cl}^-$  at one of the two adjacent high-valent iron-oxo species was more favorable than that of  $\text{H}_2\text{O}$ , resulting in the formation of an Fe–O–Cl intermediate complex (step 2). Next, considering the second-order characteristics of the hole kinetics (Fig. 3f), a concerted two-hole transfer process as the RDS contributed to the direct formation of “ $\text{Cl}^+$ ” species (*e.g.*, HClO or its equivalents), which efficiently reacted with the substrate for the Cl transfer to form the chlorination product (step 3). Then, the chlorine transfer process left a vacant  $\text{Fe}^{\text{III}}$  site on  $\alpha\text{-Fe}_2\text{O}_3$ , which was recovered by the adsorption of a  $\text{H}_2\text{O}$  molecule (step 4). In contrast, the chlorination reaction was only driven by the  $\cdot\text{Cl}$ -mediated

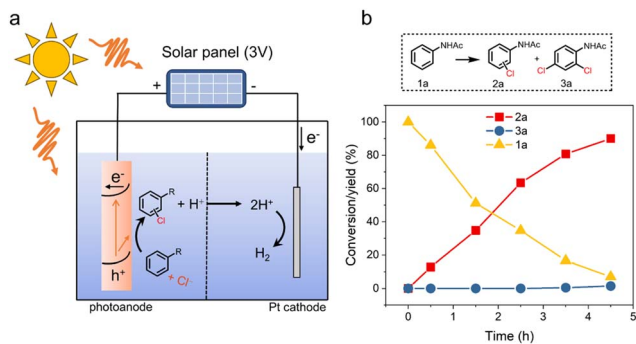


Fig. 4 The self-powered PEC system for the aromatic chlorination reaction. (a) Schematic configuration of the self-powered PEC system. (b) Time-dependent conversions of **1a** to **2a** and **3a** in the self-powered PEC system.

radical pathway on  $\text{TiO}_2$ , which resulted in low chlorination reactivity and low utilization of Cl atoms due to the uncontrolled hydrogen abstraction and polymerization side reactions.

Moreover, we also successfully constructed a self-powered PEC system for the electrophilic chlorination reaction. In this system, a solar panel ( $\sim 3\text{ V}$ ) was used to provide a constant bias (Fig. 4a). As shown in Fig. 4b, this self-powered PEC system successfully achieved aromatic chlorination of acetanilide, showing a promising approach to harness solar energy for synthesizing valuable organic halides.

## Conclusion

In this study, we report a PEC strategy for selective electrophilic chlorination reactions on  $\alpha\text{-Fe}_2\text{O}_3$  photoanodes with NaCl as the chlorine source. High selectivity (up to 99%) and faradaic efficiency (up to 90%) are achieved for the chlorination of a wide range of aromatic compounds and alkenes. A systematic PEC study verifies that the direct “ $\text{Cl}^\bullet$ ” formation process occurs on the  $\alpha\text{-Fe}_2\text{O}_3$  surface, which is facilitated by the accumulation of surface-trapped holes. The non-radical  $\text{Cl}^-$  activation characteristic and the efficient Cl transfer process make the electrophilic chlorination reactions very efficient. Moreover, we successfully constructed a self-powered PEC system for chlorinating aromatic compounds while simultaneously maintaining exceptional catalytic activity, offering a promising approach to harness solar energy for synthesizing valuable organic halides. This work provides new insight for constructing efficient chlorine atom transfer reactions by semiconductor photoelectrochemistry.

## Data availability

The authors declare that all supporting data are available in the ESI† and from the corresponding author upon request.

## Author contributions

Y. Zhang directed the project. D. Tang conceived and carried out most of the experiments. L. Wu assisted in fabricating the photoanodes and carrying out SECM measurements. Y. Zhang,

D. Tang and L. Wu wrote the manuscript, with input from others. All the authors analyzed the results and reviewed the paper.

## Conflicts of interest

There are no conflicts to declare.

## Acknowledgements

This work was supported by the National Key R&D Program of China (No. 2022YFA1505000, 2020YFC1808401), the National Natural Science Foundation of China (No. 22072158), the Strategic Priority Research Program of Chinese Academy of Sciences (No. XDB36000000) and CAS Project for Young Scientists in Basic Research (No. YSBR-004). We thank Prof. Wanhong Ma for the helpful discussions. We thank Qiaozhen Li for helping with the analysis of the products. We also express our gratitude to Jing Xue, Jiaming Wang, Siqin Liu, Kun Dang, and Dr Mingge Wu for their support in the lab. Furthermore, we would like to acknowledge the assistance provided by the staff of the 1W1B beamline at the Beijing Synchrotron Radiation Facility (BSRF) during the XAFS measurements.

## Notes and references

- 1 T. Hisatomi, J. Kubota and K. Domen, Recent advances in semiconductors for photocatalytic and photoelectrochemical water splitting, *Chem. Soc. Rev.*, 2014, **43**, 7520–7535.
- 2 C. Guo, J. Ran, A. Vasileff and S.-Z. Qiao, Rational design of electrocatalysts and photo(electro)catalysts for nitrogen reduction to ammonia ( $\text{NH}_3$ ) under ambient conditions, *Energy Environ. Sci.*, 2018, **11**, 45–56.
- 3 B. Klahr, S. Gimenez, F. Fabregat-Santiago, J. Bisquert and T. W. Hamann, Electrochemical and photoelectrochemical investigation of water oxidation with hematite electrodes, *Energy Environ. Sci.*, 2012, **5**, 7626–7636.
- 4 S. N. Habisreutinger, L. Schmidt-Mende and J. K. Stolarczyk, Photocatalytic reduction of  $\text{CO}_2$  on  $\text{TiO}_2$  and other semiconductors, *Angew. Chem., Int. Ed.*, 2013, **52**, 7372–7408.
- 5 Z. Shen, Y. Zhang, C. Zhou, J. Bai, S. Chen, J. Li, J. Wang, X. Guan, M. Rahim and B. Zhou, Exhaustive denitrification via chlorine oxide radical reactions for urea based on a novel photoelectrochemical cell, *Water Res.*, 2020, **170**, 115357.
- 6 X. Li, M. Kan, T. Wang, Z. Qin, T. Zhang, X. Qian, Y. Kuwahara, K. Mori, H. Yamashita and Y. Zhao, The  $\text{ClO}^\bullet$  generation and chlorate suppression in photoelectrochemical reactive chlorine species systems on  $\text{BiVO}_4$  photoanodes, *Appl. Catal., B*, 2021, **296**, 120387.
- 7 C.-X. Chen, S.-S. Yang, J. Ding, L. Ding, R. Wu, L.-M. Liu, J.-W. Pang, L. He, J.-Q. Jiang and N.-Q. Ren, Existence of chloride ions in high salinity wastewater accelerates the removal of micropollutants over light-driven catalysts, *Appl. Catal., B*, 2023, **334**, 122823.



- 8 X.-D. Wang, Y.-H. Huang, J.-F. Liao, Z.-F. Wei, W.-G. Li, Y.-F. Xu, H.-Y. Chen and D.-B. Kuang, Surface passivated halide perovskite single-crystal for efficient photoelectrochemical synthesis of dimethoxydihydrofuran, *Nat. Commun.*, 2021, **12**, 1202.
- 9 S. Chu, W. Li, Y. Yan, T. Hamann, I. Shih, D. Wang and Z. Mi, Roadmap on solar water splitting: current status and future prospects, *Nano Futures*, 2017, **1**, 022001.
- 10 D. Tang, K. Dang, J. Wang, C. Chen, J. Zhao and Y. Zhang, Solar-driven green synthesis of epoxides, *Sci. China: Chem.*, 2023, **66**, 3415–3425.
- 11 L. Zhang, L. Liardet, J. Luo, D. Ren, M. Grätzel and X. Hu, Photoelectrocatalytic arene C–H amination, *Nat. Catal.*, 2019, **2**, 366–373.
- 12 X. Liu, Z. Chen, S. Xu, G. Liu, Y. Zhu, X. Yu, L. Sun and F. Li, Bromide-mediated photoelectrochemical epoxidation of alkenes using water as an oxygen source with conversion efficiency and selectivity up to 100%, *J. Am. Chem. Soc.*, 2022, **144**, 19770–19777.
- 13 T. Hardwick, A. Qurashi, B. Shirinfar and N. Ahmed, Interfacial photoelectrochemical catalysis: solar-induced green synthesis of organic molecules, *ChemSusChem*, 2020, **13**, 1967–1973.
- 14 W.-Y. Fang, L. Ravindar, K. P. Rakesh, H. M. Manukumar, C. S. Shantharam, N. S. Alharbi and H.-L. Qin, Synthetic approaches and pharmaceutical applications of chloro-containing molecules for drug discovery: A critical review, *Eur. J. Med. Chem.*, 2019, **173**, 117–153.
- 15 S. Engbers, R. Hage and J. E. M. N. Klein, Toward environmentally benign electrophilic chlorinations: from Chloroperoxidase to bioinspired Isoporphyrins, *Inorg. Chem.*, 2022, **61**, 8105–8111.
- 16 S. Han, C. Cheng, M. He, R. Li, Y. Gao, Y. Yu, B. Zhang and C. Liu, Preferential adsorption of ethylene oxide on Fe and chlorine on Ni enabled scalable electrocatalysis of ethylene chlorohydrin, *Angew. Chem., Int. Ed.*, 2023, **62**, e202216581.
- 17 X. Wang, Z. Chen, Q. Liu, W. Lin and X. Xiong, Amine organocatalysts for highly ortho-selective chlorination of anilines with sulfonyl chloride, *Chem. Commun.*, 2022, **58**, 13325–13328.
- 18 L. Zhang and X. Hu, Room temperature C(sp<sup>2</sup>)-H oxidative chlorination via photoredox catalysis, *Chem. Sci.*, 2017, **8**, 7009–7013.
- 19 F. Liu, N. Wu and X. Cheng, Chlorination reaction of aromatic compounds and unsaturated carbon-carbon bonds with chlorine on demand, *Org. Lett.*, 2021, **23**, 3015–3020.
- 20 L. Huang, P. Wang, Y. Jiang, K. Davey, Y. Zheng and S.-Z. Qiao, Ethylene electrooxidation to 2-chloroethanol in acidic seawater with natural chloride participation, *J. Am. Chem. Soc.*, 2023, **145**, 15565–15571.
- 21 M. Chung, K. Jin, J. S. Zeng and K. Manthiram, Mechanism of chlorine-mediated electrochemical ethylene oxidation in saline water, *ACS Catal.*, 2020, **10**, 14015–14023.
- 22 W. R. Leow, Y. Lum, A. Ozden, Y. Wang, D.-H. Nam, B. Chen, J. Wicks, T.-T. Zhuang, F. Li, D. Sinton and E. H. Sargent, Chloride-mediated selective electrocatalysis of ethylene and propylene oxides at high current density, *Science*, 2020, **368**, 1228–1233.
- 23 Y. Liang, F. Lin, Y. Adeli, R. Jin and N. Jiao, Efficient electrocatalysis for the preparation of (hetero)aryl chlorides and vinyl chloride with 1,2-dichloroethane, *Angew. Chem., Int. Ed.*, 2019, **58**, 4566–4570.
- 24 P. Zhang, T. Wang and J. Gong, Advances in electrochemical oxidation of olefins to epoxides, *CCS Chem.*, 2023, **5**, 1028–1042.
- 25 Z. Li, L. Luo, M. Li, W. Chen, Y. Liu, J. Yang, S.-M. Xu, H. Zhou, L. Ma, M. Xu, X. Kong and H. Duan, Photoelectrocatalytic C–H halogenation over an oxygen vacancy-rich TiO<sub>2</sub> photoanode, *Nat. Commun.*, 2021, **12**, 6698.
- 26 G. Zhang, J. Ruan and T. Du, Recent advances on photocatalytic and electrochemical oxidation for ammonia treatment from water/wastewater, *ACS ES&T Engg*, 2021, **1**, 310–325.
- 27 J. Ye, D. Zhang, S. Salli, Y. Li, F. Han, Y. Mai, F. Rosei, Y. Li, Y. Yang, F. Besenbacher, H. Niemantsverdriet, E. Richards and R. Su, Heterogeneous photocatalytic recycling of FeX<sub>2</sub>/FeX<sub>3</sub> for efficient halogenation of C–H bonds using NaX, *Angew. Chem., Int. Ed.*, 2023, **62**, e202302994.
- 28 P. Xu, P.-Y. Chen and H.-C. Xu, Scalable photoelectrochemical dehydrogenative cross-coupling of heteroarenes with aliphatic C–H bonds, *Angew. Chem., Int. Ed.*, 2020, **59**, 14275–14280.
- 29 M. Xiang, C. Zhou, X.-L. Yang, B. Chen, C.-H. Tung and L.-Z. Wu, Visible light-catalyzed benzylic C–H bond chlorination by a combination of organic dye (Acr<sup>+</sup>-Mes) and N-chlorosuccinimide, *J. Org. Chem.*, 2020, **85**, 9080–9087.
- 30 Y. Zhao, C. Deng, D. Tang, L. Ding, Y. Zhang, H. Sheng, H. Ji, W. Song, W. Ma, C. Chen and J. Zhao,  $\alpha$ -Fe<sub>2</sub>O<sub>3</sub> as a versatile and efficient oxygen atom transfer catalyst in combination with H<sub>2</sub>O as the oxygen source, *Nat. Catal.*, 2021, **4**, 684–691.
- 31 L. Wu, D. Tang, J. Xue, S. Liu, J. Wang, H. Ji, C. Chen, Y. Zhang and J. Zhao, Competitive non-radical nucleophilic attack pathways for NH<sub>3</sub> oxidation and H<sub>2</sub>O oxidation on hematite photoanodes, *Angew. Chem., Int. Ed.*, 2022, **61**, e202214580.
- 32 O. Zandi and T. W. Hamann, Determination of photoelectrochemical water oxidation intermediates on hematite electrode surfaces using operando infrared spectroscopy, *Nat. Chem.*, 2016, **8**, 778–783.
- 33 B. Klahr and T. Hamann, Water oxidation on hematite photoelectrodes: Insight into the nature of surface states through in situ spectroelectrochemistry, *J. Phys. Chem. C*, 2014, **118**, 10393–10399.
- 34 F. Le Formal, E. Pastor, S. D. Tilley, C. A. Mesa, S. R. Pendlebury, M. Grätzel and J. R. Durrant, Rate law analysis of water oxidation on a Hematite surface, *J. Am. Chem. Soc.*, 2015, **137**, 6629–6637.
- 35 T. Takashima, K. Ishikawa and H. Irie, Detection of intermediate species in oxygen evolution on Hematite

- electrodes using spectroelectrochemical measurements, *J. Phys. Chem. C*, 2016, **120**, 24827–24834.
- 36 C. A. Mesa, L. Francàs, K. R. Yang, P. Garrido-Barros, E. Pastor, Y. Ma, A. Kafizas, T. E. Rosser, M. T. Mayer, E. Reisner, M. Grätzel, V. S. Batista and J. R. Durrant, Multihole water oxidation catalysis on haematite photoanodes revealed by operando spectroelectrochemistry and DFT, *Nat. Chem.*, 2020, **12**, 82–89.
- 37 F. H. Vaillancourt, E. Yeh, D. A. Vosburg, S. Garneau-Tsodikova and C. T. Walsh, Nature's inventory of halogenation catalysts: oxidative strategies predominate, *Chem. Rev.*, 2006, **106**, 3364–3378.
- 38 H.-A. Wagenknecht and W.-D. Woggon, New active-site analogues of Chloroperoxidase—syntheses and catalytic reactions, *Angew. Chem., Int. Ed.*, 1997, **36**, 390–392.
- 39 Z. Cong, S. Yanagisawa, T. Kurahashi, T. Ogura, S. Nakashima and H. Fujii, Synthesis, characterization, and reactivity of hypochloritoiron(III) porphyrin complexes, *J. Am. Chem. Soc.*, 2012, **134**, 20617–20620.
- 40 Z. Cong, T. Kurahashi and H. Fujii, Oxidation of chloride and subsequent chlorination of organic compounds by oxoiron(IV) porphyrin  $\pi$ -cation radicals, *Angew. Chem., Int. Ed.*, 2011, **50**, 9935–9939.
- 41 Y. Yao, L. Zhao, J. Dai, J. Wang, C. Fang, G. Zhan, Q. Zheng, W. Hou and L. Zhang, Single atom Ru monolithic electrode for efficient chlorine evolution and nitrate reduction, *Angew. Chem., Int. Ed.*, 2022, **61**, e202208215.
- 42 C. Y. Cummings, F. Marken, L. M. Peter, K. G. Upul Wijayantha and A. A. Tahir, New insights into water splitting at mesoporous  $\alpha$ -Fe<sub>2</sub>O<sub>3</sub> films: a study by modulated transmittance and impedance spectroscopies, *J. Am. Chem. Soc.*, 2012, **134**, 1228–1234.
- 43 B. Klahr, S. Gimenez, F. Fabregat-Santiago, T. Hamann and J. Bisquert, Water oxidation at hematite photoelectrodes: the role of surface states, *J. Am. Chem. Soc.*, 2012, **134**, 4294–4302.
- 44 Y. Zhang, H. Zhang, A. Liu, C. Chen, W. Song and J. Zhao, Rate-limiting O–O bond formation pathways for water oxidation on Hematite photoanode, *J. Am. Chem. Soc.*, 2018, **140**, 3264–3269.
- 45 Y. Zhang, H. Zhang, H. Ji, W. Ma, C. Chen and J. Zhao, Pivotal role and regulation of proton transfer in water oxidation on hematite photoanodes, *J. Am. Chem. Soc.*, 2016, **138**, 2705–2711.
- 46 T. Hering, B. Mühlendorf, R. Wolf and B. König, Halogenase-inspired oxidative chlorination using flavin photocatalysis, *Angew. Chem., Int. Ed.*, 2016, **55**, 5342–5345.
- 47 N. Fu, G. S. Sauer and S. Lin, Electrocatalytic radical dichlorination of alkenes with nucleophilic chlorine sources, *J. Am. Chem. Soc.*, 2017, **139**, 15548–15553.
- 48 N. Fu, G. S. Sauer, A. Saha, A. Loo and S. Lin, Metal-catalyzed electrochemical diazidation of alkenes, *Science*, 2017, **357**, 575–579.
- 49 Q. Wang, T. Li, C. Yang, M. Chen, A. Guan, L. Yang, S. Li, X. Lv, Y. Wang and G. Zheng, Electrocatalytic methane oxidation greatly promoted by chlorine intermediates, *Angew. Chem., Int. Ed.*, 2021, **60**, 17398–17403.
- 50 Z. Shen, J. Li, Y. Zhang, J. Bai, X. Tan, X. Li, L. Qiao, Q. Xu and B. Zhou, Highly efficient total nitrogen and simultaneous total organic carbon removal for urine based on the photoelectrochemical cycle reaction of chlorine and hydroxyl radicals, *Electrochim. Acta*, 2019, **297**, 1–9.
- 51 C. A. Mesa, L. Francàs, K. R. Yang, P. Garrido-Barros, E. Pastor, Y. Ma, A. Kafizas, T. E. Rosser, M. T. Mayer, E. Reisner, M. Grätzel, V. S. Batista and J. R. Durrant, Multihole water oxidation catalysis on haematite photoanodes revealed by operando spectroelectrochemistry and DFT, *Nat. Chem.*, 2020, **12**, 82–89.